# Flow structure, heat transfer and scaling analysis in the case of thermo-magnetic convection in a differentially heated cylindrical enclosure



Journal of Physics: Conference Series **530** (2014) 012041 doi:10.1088/1742-6596/530/1/012041

# Flow structure, heat transfer and scaling analysis in the case of thermo-magnetic convection in a differentially heated cylindrical enclosure

**E Fornalik-Wajs[1], P Filar[2], J Wajs[3], A Roszko[1], L Pleskacz[1] and H Ozoe[4]**
[1] AGH University of Science and Technology, Department of Fundamental Research in Energy Engineering, Al. Mickiewicza 30, 30-059 Krakow, Poland
[2] Siltronic AG, Hanns-Seidel-Platz 4, 81737 München, Germany
[3] Gdansk University of Technology, Department of Energy and Industrial Apparatus, ul. Narutowicza 11/12, 80-233 Gdansk, Poland
[4] Professor Emeritius of Kyushu University, Kasuga Koen 6 1, 816 8580 Fukuoka, Japan

E-mail: roszko@agh.edu.pl

**Abstract.** The experimental, numerical and scaling analysis in the case of thermo-magnetic convection in a thermosyphon-like enclosure filled with a paramagnetic fluid is presented. Visualization of temperature field together with the numerical simulation gave an information about the flow structure, which indicated "finger-like" structures of hot and cold streams advecting each other. Their number depended on the Rayleigh number and also on the magnetic induction. In the basis of thermal measurements the average Nusselt number was determined for various strength of magnetic field and in presented configuration increasing magnetic field caused increase in the Nusselt number. With the assumptions of two dimensional flow and the constant fluid properties, in the studied temperature range, the scaling analysis led to the Nusselt number correlation in dependence on the thermo-magnetic Rayleigh number. Very good agreement between the experimental results and scaling equation was observed.

## 1. Introduction

Closed thermosyphon has a wide range of applications, for example cooling thermal devices (i.e. gas turbine blades [1]), or more specified like preserving permafrost under the buildings or modeling the temperature distribution in earth drillings [2]. Thermosyphons were studied to gain a fundamental understanding of phenomena occurring in such geometry and its comprehensive experimental and numerical studies can be found in [1,2,3,4]. Researchers applied various experimental and numerical approaches, which were mainly related to the applications of thermosyphon. The results show the specific flow pattern in the middle-height cross-section. The appearance of the "streams"/"branches" (in this paper they are called "spokes") of cold and hot fluid advected to each other was noticed. This phenomenon had an influence on the heat transfer between the two streams. In [1] it was stated that the heat transfer can be enhanced "when the earth's gravitational field… is replaced by more powerful body force fields…", for example magnetizing force.

The additional source of acceleration due to a strong magnetic field was introduced to many studied systems, for example in chemistry [5], physics [6], medicine [7], engineering [8]. The new phenomena

were found, for example levitation of various materials in a strong magnetic field, magnetic breath support, magneto-thermal wind, enhanced oxygen supply for the fuel cell [9,10]. Very interesting analysis showing intensification of the heat transfer processes by the magnetic field in the cubical [11, 12], annular [13] and thermosyphon-like geometry was reported in [14].
In the presented paper the experimental and numerical analysis of magneto-convection in the thermosyphon-like enclosure is complemented with scaling analysis.

## 2. Experimental apparatus

The experimental setup consisted of the magnet, analyzed enclosure, constant temperature bath, temperature data acquisition system, computer, power supply unit and its control system. The cylindrical enclosure (figure 1) consisted of the heating and cooling side walls, with the height of 0.028 m, made of copper and separated by the Plexiglas adiabatic interface of width 0.004 m. The top and bottom end plates of the cylinder were made of Plexiglas and the enclosure was filled with the 50% volume aqueous solution of glycerol. A nichrome wire, covered by rubber, was winded at the outside surface of the cylinder to heat one part of the enclosure. The wire was connected to a DC power supply controlled by the multimeters. The second copper part consisted of a small chamber through which thermostating water was pumped to keep the cooled side wall at constant temperature. The temperature difference was measured with the T-type thermocouples (marked in figure 1 as T.C.). Two thermocouples were located on the outer side of the heated wall while another two were attached to the outlet and inlet of coolant. The working fluid was illuminated through the middle-height adiabatic zone by a white light sheet from the high luminosity LED diodes placed inside the holes drilled in the Plexiglas adiabatic zone. Pictures were taken through the top Plexiglas plate.

## 3. Properties of the working fluid

The 50% aqueous solution of glycerol was chosen as the working fluid. Its density was measured with a pycnometer and viscosity with an Ostwald's viscosimeter. Other properties marked with the asterisk in Table 1 were estimated from [15]. The Prandtl number ($Pr = \nu/\alpha$) of the working fluid was estimated on the basis of the fluid properties and was equal to Pr = 42.1. The mass magnetic susceptibility $\chi_g$ of the working fluid was measured with the magnetic susceptibility balance according to the modified Gouy method (Evan's method) and was equal to $+35\times10\text{-}8[m^3/kg]$.

**Table 1.** Properties of 50% aqueous solution of glycerol at $T_0$ = 298[K] (the properties marked by asterisk were estimated from [15]).

| Property | Value | Unit |
|---|---|---|
| $\alpha$* | = 1.1415×10-7 | $m^2/s$ |
| $\beta$* | = 0.445×10-3 | $K^{-1}$ |
| $\lambda$* | = 0.422 | W/(m·K) |
| $\eta$ | = 6.145×10-3± 0.064×10-3 | Pa·s |
| $\nu$ | = 4.80×10-6 ± 0.05×10-6 | $m^2/s$ |
| $\rho_0$ | = 1281± 1 | $kg/m^3$ |
| $\chi_{g0}$ | = 13.926×10-8± 0.329×10-8 | $m^3/kg$ |

## 4. Experimental procedure

The experimental setup, insulated by a vinyl foil, was placed into the bore of the HF5-100VHT helium free 5 T superconducting magnet. It was placed in the bore in such position that the middle-height level of an enclosure was placed at 0.1 m from one of the bore ends. That level assured that the radial component of the magnetic force would be minimal. The distribution of the axial component of magnetic force is presented in figure 2(a), while the vectors represent the magnetic force vectors

acting on the enclosure placed in the bore of the superconducting magnet in figure 2(b). The visualization of fluid temperature was carried out with an encapsulated liquid crystal slurry, illuminated with the LED's white light. Detailed description of experimental procedure is presented in [14]. The Rayleigh number was very important in the analysis. In the papers related to the thermosyphons, the inner radius [2] or the diameter [4] of the enclosure were considered as the characteristic length. The radius of the enclosure was chosen as the characteristic length in the presented studies, and therefore the Rayleigh number took the form

$$\mathrm{Ra} = g\beta\left(T_\mathrm{h} - T_\mathrm{c}\right) r_0^3 (\alpha\nu)^{-1}, \tag{1}$$

where $g$ means the gravitational acceleration, $\beta$ indicates the thermal expansion coefficient, $T_\mathrm{h}$ denotes temperature of heated enclosure part, while $T_\mathrm{c}$ temperature of cooled one, $r_0$ is the enclosure radius, $\alpha$ means the thermal diffusivity and $\nu$ is the kinematic viscosity.

The magnetic Rayleigh number applied in this paper was based on Braithwaite's definition [16] and adopted to the studied cases. Finally it took form:

$$\mathrm{Ra}_\mathrm{m} = \mathrm{Ra}\left[1 + \chi_{\mathrm{g}0} C_\mathrm{n} (g\mu_0)^{-1} \left(\boldsymbol{B}\nabla\boldsymbol{B}\right)\right], \tag{2}$$

where Ra means the thermal Rayleigh number, $\chi_{\mathrm{g}0}$ is the mass magnetic susceptibility, $C_\mathrm{n} = 1+1/(\beta T_0)$, $\mu_0$ is the magnetic permeability of vacuum and $\boldsymbol{B}$ represents the magnetic induction.

## 5. Heat transfer rate

The thermal measurements were carried out to investigate the influence of magnetic field on the flow structure and indirectly on the heat transfer rate. Definition of the Nusselt number was

$$\mathrm{Nu} = \dot{Q}_\mathrm{net\_conv} \cdot \dot{Q}_\mathrm{net\_cond}^{-1}. \tag{3}$$

The net conduction ($\dot{Q}_\mathrm{net\_cond}$) and net convection ($\dot{Q}_\mathrm{net\_conv}$) heat fluxes were estimated according to the method invented in [17]. The definitions of net conduction heat and net convection heat fluxes were formulated as

$$\dot{Q}_\mathrm{net\_cond} = \dot{Q}_\mathrm{cond} - \dot{Q}_\mathrm{loss}, \tag{4}$$

$$\dot{Q}_\mathrm{net\_conv} = \dot{Q}_\mathrm{conv} - \dot{Q}_\mathrm{loss}. \tag{5}$$

Heat loss was assumed to depend on the heater temperature itself and not on the mode of heat transfer inside the enclosure.

The empty thermosyphon-like enclosure was placed into the bore of the magnet and the heat loss ($\dot{Q}_\mathrm{loss}$) to the environment was measured. It was assumed that the convection and conduction of the air were negligible due to its low thermal conductivity.

Because of the complex geometry of the experimental system, the net conduction flux in the working fluid ($\dot{Q}_\mathrm{net\_cond}^\mathrm{fluid}$) was difficult to measure. In the thermosyphon placed upside down (the upper side wall was heated and the lower side wall cooled) the convection occurred near the side walls. Therefore a jelly was used to obtain the conduction state in the cylindrical enclosure. In the solidified jelly, the heat transfer took place only by conduction. After the measurement of the conduction through the jelly, the conduction heat flux through the working fluid for the same system was presumed to be approximated by the equation

$$\dot{Q}_\mathrm{net\_cond}^\mathrm{fluid} = \dot{Q}_\mathrm{net\_cond}^\mathrm{jelly} \cdot \lambda^\mathrm{fluid} \cdot (\lambda^\mathrm{jelly})^{-1}. \tag{6}$$

The estimated value of the thermal conductivity of the jelly was $\lambda^\mathrm{jelly} = 0.575 \pm 0.40$ W/(m·K).

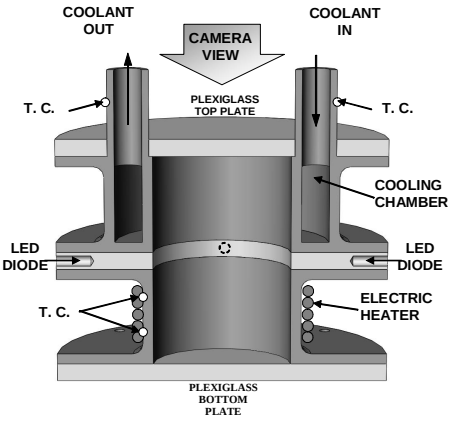


**Figure 1.** Schematic view of the experimental apparatus.

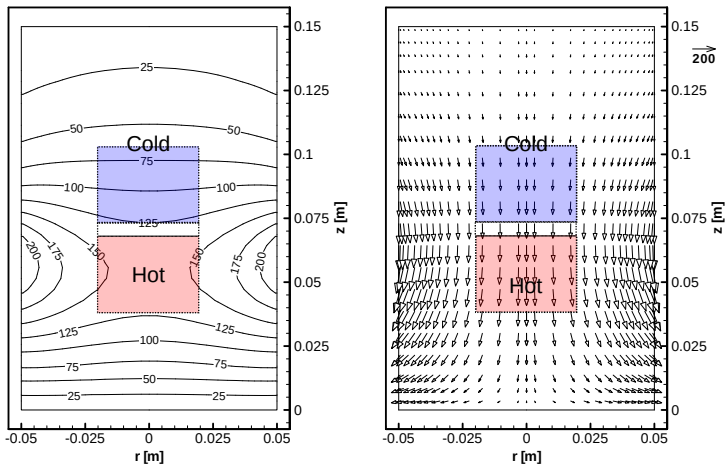


**Figure 2.** Calculated distribution of (a) axial component of the magnetic force $B_z$ $(\partial B_z/\partial z)$; (b) gradient of square of magnetic induction $\nabla B^2$ at the maximal magnetic induction of 5 T.

## 6. Numerical analysis

The numerical approach was based on the model for the magnetic convection of a paramagnetic fluid proposed in [18]. The fluid was assumed to be Newtonian, incompressible and the Boussinesq approximation was employed. The analyzed problem was three-dimensional. The governing equations can be written as follows in non-dimensional form:
continuity equation:

$$\nabla \cdot \boldsymbol{V}_{\mathbf{n}} = 0\,, \tag{7}$$

momentum equation:

$$\frac{D\boldsymbol{V}_{\mathbf{n}}}{D\tau_{\mathrm{n}}} = -\nabla P_{\mathrm{n}} + \mathrm{Pr}\nabla^2 \boldsymbol{V}_{\mathbf{n}} + \mathrm{Ra}\,\mathrm{Pr}\,T_{\mathrm{n}}\left[1 - 0.5\gamma C_{\mathrm{n}} \nabla B_{\mathrm{n}}^2\right], \tag{8}$$

energy equation:

$$\frac{DT_{\mathrm{n}}}{D\tau_{\mathrm{n}}} = \nabla^2 T_{\mathrm{n}}\,, \tag{9}$$

Biot-Savart's law:

$$\boldsymbol{B_n} = \frac{1}{4\pi} \oint_{solenoid} \frac{\boldsymbol{dS_{nl}} \times \boldsymbol{R}}{R^3}\,. \tag{10}$$

The non-dimensional al variables were defined as follows [16] $\boldsymbol{V}_{\mathrm{n}} = v/v_0$, $v_0 = \alpha/r_0$, $S_{\mathrm{nl}} = s_{\mathrm{l}}/r_0$, $R = r/r_0$, $B_0 = \mu_0 i/r_0$, $\tau_{\mathrm{n}} = t/t_0$, $P_{\mathrm{n}} = p/p_0$, $\boldsymbol{B}_{\mathbf{n}} = B/B_0$, $T_{\mathrm{n}} = (T - T_0)/(T_{\mathrm{h}} - T_{\mathrm{c}})$, $t_0 = r_0^2/\alpha$, $p_0 = \rho_0\alpha^2/r_0^2$, $p_0 = \rho_0\alpha^2/l^2$, $T_0 = (T_{\mathrm{h}} + T_{\mathrm{c}})/2$, $C_{\mathrm{n}} = 1 + 1/(\beta T_0)$, $\mathrm{Pr} = \nu/\alpha$, $\mathrm{Ra} = g\beta(T_{\mathrm{h}} - T_{\mathrm{c}})r_0^3/(\alpha\nu)$, $\gamma = \chi_0 B_0^2/(\rho_0\mu_{\mathrm{m}} g r_0)$.
The above partial differential equations were approximated by the finite difference equations. The HSMAC (**H**ighly **S**implified **M**arker **A**nd **C**ell) method with the third-order upwind scheme applied for the inertial terms was used to iterate mutually the pressure and the velocity field. The magnetic field was computed using Biot-Savart's law for the multi-coil system. It was done in such way to simulate specific distribution of the magnetic field as that generated by the solenoid in the real system. Numerical computations were carried out for the same conditions as the experiment and the dimensionless parameters were computed from the experimental conditions and the properties of the fluid.

## 7. Results

The enclosure was heated from the lower side wall and cooled from the upper one therefore the convection occurred even without a magnetic field. The experimental analysis was done for various values of Rayleigh number. These results were reported in [19], however it can be said that increasing Rayleigh number caused increase in the number of "spokes/branches" in the same way as the magnetic field does, because in the presented configurations the gravitational and magnetizing forces acts in the same direction and as a result the enhanced convection is obtained.

Figure 3 shows the experimental and calculated results at thermal Rayleigh number Ra = $1.69\times10^5$ and the magnetic field of 0 T. Figure 3(a) presents the image of isotherms with five spoke pattern taken in the middle-height cross-section. Figure 3(b) shows the calculated temperature field and the velocity vectores at the cylinder middle-height. Five spokes of red/yellow color (representing the cold fluid) and five bluish (representing the hot fluid) placed alternatively along the perimeter of cross-section could be counted. They correspond to the five blue and five red spokes presented in figure 3(a).

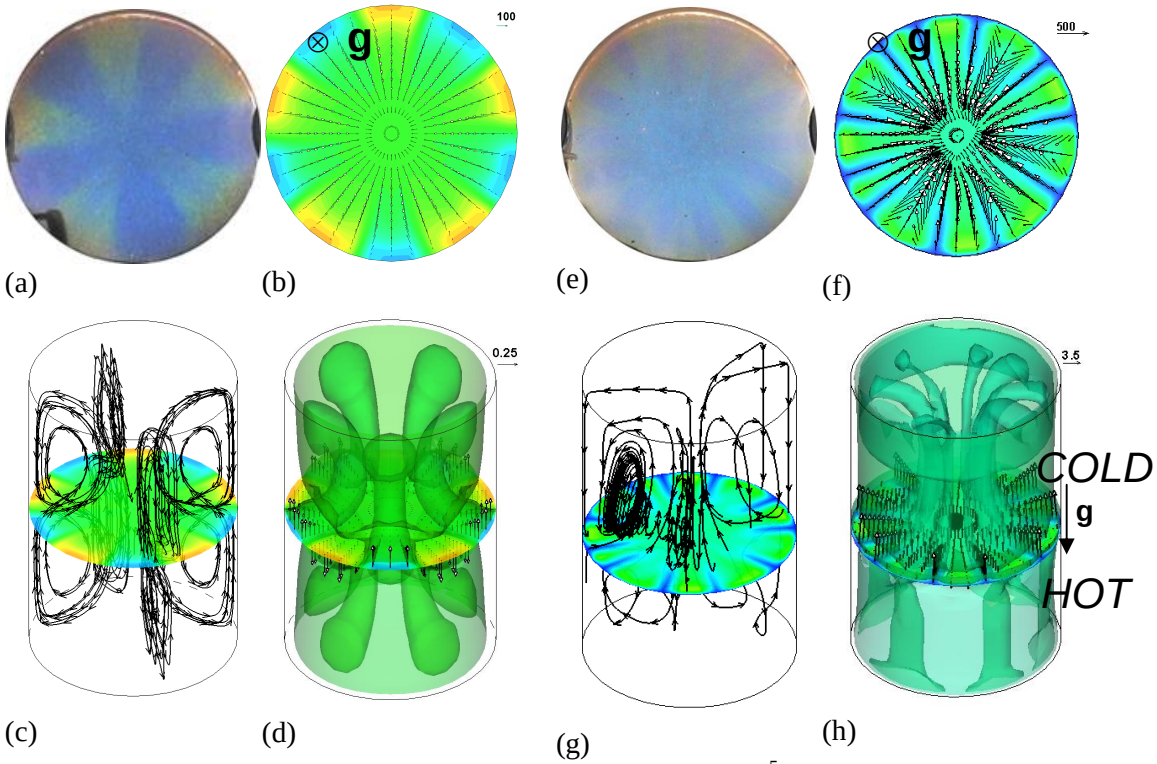


**Figure 3.** The results at thermal Rayleigh number Ra = 1. $69\times10^5$ and $B_0$ = 0 T: (a) visualized temperature field, (b) computed temperature field with velocity vectors, (c) calculated temperature field at cylinder mid-height and long time streak lines, (d) isothermal surfaces and the gravitational buoyancy force vectors [19]; The results at thermal Rayleigh number Ra = $1.43\times10^5$ and $B_0$ = 5 T: (e) visualized temperature field, (f) computed temperature field with velocity vectors, (g) calculated temperature field and long time streak lines, (h) isothermal surfaces and the total force vectors.

Figure 3(c) shows calculated temperature field at the cylinder middle-height cross-section with the three-dimensional demonstration of long time streak lines starting from four different angular positions. The fluid moved upwards near the lower heated side wall, then proceeded toward the enclosure centre at the middle-height and near the centre ascended toward the top of cylinder. Finally, fluid descended along the upper cooled side wall. This trajectory is typical for the thermosyphon systems and was reported in [2,3]. Figure 3(d) shows the finger-like isothermal surfaces of $T_n$ = -0.05 and $T_n$ = 0.05 and the gravitational buoyancy force vectors $\boldsymbol{F_g}$ drawn at the cylinder's middle-height.

The isothermal contours correspond to the five spoke patterns obtained at the middle-height level of the enclosure.
Afterwards the calculations were carried out at the magnetic induction level of 1T, 2T, 3T, 4T and 5T, however only the results for the highest value are presented here. Increasing magnetic induction strengthened the magnetizing force and the number of spokes increased. Their shape became less regular and led to the state presented in figures 3(e-h).
Figure 3 presents also the experimental and computed results at Ra = $1.43\times10^5$ and 5 T of the magnetic induction. Figure 3(e) presents the visualized temperature field with a fourteen spoke pattern taken in the middle-height cross-section. In Figure 3(f) the eleven green (cold fluid) and blue (hot fluid) spokes can be counted in the computed result. There is some discrepancy in the number of spokes observed in figures 3(e) and 3(f). The shown computed cross-section was at the level Z = 1.7. Figure 3(g) shows calculated temperature field at the level Z = 1.7 with the three-dimensional demonstration of long time streak lines starting from four different angular positions. Figure 3(h) shows the isothermal surfaces of $T_n = 0.12$ and $T_n = 0.193$ and the total force vectors $\boldsymbol{F}_\mathbf{m} + \boldsymbol{F}_\mathbf{g}$ drawn at the cylinder middle-height. The finger-shape isothermal surfaces become very distorted. It is also observed that they moved toward the centre of the enclosure and toward the side-walls, which can be compared with the thickening of the boundary layer with an increase in the Rayleigh number.

## 8. Scaling analysis

The conservation of mass equation for two-dimensional flow in a thermosyphon-like enclosure filled with incompressible fluid can be written in dimensional form as

$$\frac{\partial v_z}{\partial z} + \frac{1}{r}\frac{\partial}{\partial r}\left(r v_r\right) = 0 . \tag{11}$$

The momentum equations in incompressible fluid with the assumption of constant viscosity in terms of scalar components can be expressed as

$$\frac{\partial v_z}{\partial t} + v_z\frac{\partial v_z}{\partial z} + v_r\frac{\partial v_z}{\partial r} = -\frac{1}{\rho}\frac{\partial p'}{\partial z} + \nu\left(\frac{1}{r}\frac{\partial}{\partial r}\left(r\frac{\partial v_z}{\partial r}\right) + \frac{\partial^2 v_z}{\partial z^2}\right) - \frac{\chi_{g0}\beta C_n}{2\mu_0}\left(T - T_0\right)\frac{\partial B^2}{\partial z} + \beta\left(T - T_0\right)\mathbf{g} \tag{12}$$

$$\frac{\partial v_r}{\partial t} + v_z\frac{\partial v_r}{\partial z} + v_r\frac{\partial v_r}{\partial r} = -\frac{1}{\rho}\frac{\partial p'}{\partial r} + \nu\left(\frac{1}{r}\frac{\partial}{\partial r}\left(r\frac{\partial v_r}{\partial r}\right) - \frac{v_r}{r^2} + \frac{\partial^2 v_r}{\partial z^2}\right) - \frac{\chi_{g0}\beta C_n}{2\mu_0}\left(T - T_0\right)\frac{\partial B^2}{\partial r} . \tag{13}$$

The energy equation applied in the numerical analysis can be presented as

$$\frac{\partial T}{\partial t} + v_z\frac{\partial T}{\partial z} + v_r\frac{\partial T}{\partial r} = \alpha\left(\frac{1}{r}\frac{\partial}{\partial r}\left(r\frac{\partial T}{\partial r}\right) + \frac{\partial^2 T}{\partial z^2}\right). \tag{14}$$

Instead of solving equations (11-14) numerically, the scaling analysis can be done to predict theoretically the types of flow and heat transfer patterns that can develop in the enclosure. Immediately after $t = 0$, the fluid in the vicinity of side wall is motionless: this means that near the side wall the energy equation (14) expresses a balance between thermal inertia and conduction normal to the wall [20]

$$\frac{\Delta T}{t} \approx \alpha\frac{\Delta T}{\delta_T^2} . \tag{15}$$

This equality of scales follows from recognizing $\Delta T$, $t$ and $\delta_T$ as the scales of changes in $T$, $t$ and $r$ in equation (14). In the same equation $v_z = v_r = 0$, also $\partial^2 T/\partial z^2 << \partial^2 T/\partial r^2$, because near $t = 0^+$ the thermal boundary layer thickness $\delta_T$ is much smaller than the enclosure height ($z \sim l$, where $l=h/2$ and $r \sim \delta_T$). Equation (15) shows that in the time immediately following $t = 0$, each side wall is coated with a conduction layer whose thickness increases steadily as

$$\delta_{\mathrm{T}} \approx (\alpha t)^{1/2}. \tag{16}$$

The heated layer $\delta_{\mathrm{T}}$ will naturally tend to rise along the heated wall. To find the velocity scale of this upward motion $v$, the momentum could be divided into three terms: inertia, friction and buoyancy, respectively in equation (17). In terms of representative scales, the momentum balance can be read

$$\frac{v_r}{\delta_T t}, \qquad \nu \frac{v_r}{{\delta_T}^3} \quad \approx \quad \frac{\chi_{\mathrm{g0}} \beta C_n}{2\mu_0} \frac{\Delta T}{\delta_T} \frac{B_0^2}{l} + \boldsymbol{g}\beta \frac{\Delta T}{\delta_T}. \tag{17}$$

The driving force in the momentum balance is the buoyancy effect caused by the gravitational and magnetizing forces. It can be found whether the buoyancy effect is balanced by friction or inertia. For fluids with a Prandtl number equal 1 or more, the momentum balance at $t = 0^+$ is between buoyancy and friction

$$1 \approx \frac{\chi_{\mathrm{g0}} \beta C_n}{2\mu_0} \frac{\Delta T B_0^2 \delta_T^2}{l \nu_r} + \boldsymbol{g}\beta \frac{\Delta T \delta_T^2}{\nu \nu_r}. \tag{18}$$

The initial vertical velocity scale is

$$v_r \approx \frac{\boldsymbol{g}\beta \Delta T \delta_T^2}{\nu} \left( 1 + \frac{\chi_{\mathrm{g0}} C_n}{2\boldsymbol{g}\mu_0} \frac{B_0^2}{l} \right). \tag{19}$$

The heat conducted from the side wall into the fluid layer $\delta_{\mathrm{T}}$ is no longer spent on thickening the layer: part of this heat input is carried away by the layer $\delta_{\mathrm{T}}$ rising with velocity $v_r$ [20]. In the energy equation three effects can be considered: inertia, convection and conduction. At final time $t_{\mathrm{f}}$ the energy equation expresses a balance between the heat conducted from the wall and the enthalpy carried away vertically by the buoyant layer

$$v_r \frac{\Delta T}{l} \quad \approx \quad \alpha \frac{\Delta T}{\delta_T^2}, \tag{20}$$

which thickness can be described by equation (16), therefore

$$\delta_{\mathrm{T,f}} \approx l \left[ \frac{\boldsymbol{g}\beta \Delta T l^3}{\nu \alpha} \left( 1 + \frac{\chi_{\mathrm{g0}} C_{\mathrm{n}}}{2\boldsymbol{g}\mu_0} \frac{B_0^2}{l} \right) \right]^{-1/4}, \tag{21}$$

it can also be written

$$\delta_{\mathrm{T,f}} \approx l \left[ \mathrm{Ra} \left( 1 + 0.5 \gamma C_{\mathrm{n}} \right) \right]^{-1/4} = l \left( \mathrm{Ra}_{\mathrm{m}} \right)^{-1/4}, \tag{22}$$

$C_n$ is a constant and $\mathrm{Ra_m}$ is the magnetic Rayleigh number (equation (2)).
Using the convective heat transfer coefficient, the following relation can be written for the studied case

$$\alpha \Delta T \approx \lambda \frac{\Delta T}{\delta_{\mathrm{T}}}. \tag{23}$$

The order of magnitude for the average Nusselt number is

$$\mathrm{Nu} \approx \frac{\alpha l}{\lambda} \approx \frac{l}{\delta_{\mathrm{T}}} \approx \left( \mathrm{Ra}_{\mathrm{m}} \right)^{1/4}. \tag{24}$$

The results are presented in figure 4 in comparison with the experimental data. The assumption about two-dimensional flow was made. The final relation between the Nusselt number and the magnetic Rayleigh number presented as equation (24) was applied, especially because the magnetic Rayleigh number was already used to characterize the flow in the thermosyphon-like enclosure under the magnetic field.

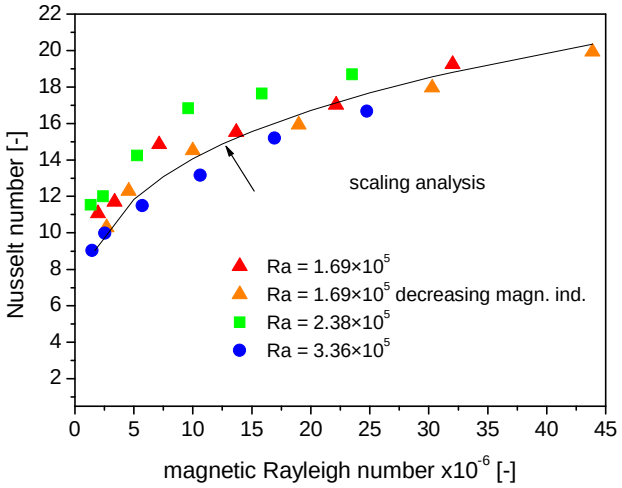


**Figure 4.** Relation between the Nusselt and the magnetic Rayleigh numbers coming from experimental and scaling analysis for the cylindrical thermosyphon-like enclosure at thermal Rayleigh number values ▲▲Ra = $1.69\times10^5$, ■Ra = $2.38\times10^5$, ●Ra = $3.36\times10^5$ and various magnetic inductions

Good correspondence between the experimental data and scaling law can be observed in figure 4, even with the applied assumptions. Some differences between the presented experimental and numerical data and the results of scaling analysis can derive from the assumptions about the two-dimensionality of the flow, when the real flow is three-dimensional. The accuracy of the measurements and simplification of the conservation laws could have an influence on the scaling analysis. Ultimately, the most important point is that this analysis is suitable for brief and quick prediction of the Nusselt number.

## 9. Summary

Combined effect of thermal buoyancy force and magnetic field on the fluid behavior in the thermosyphon-like enclosure was presented. Gravitational and magnetizing forces were acting in the same direction, therefore increasing Rayleigh number and increasing magnetic field resulted in the enhanced heat transfer. It could be observed by increasing number of "spokes" and increasing value of Nusselt number. Very interesting flow structure was obtained numerically and compared with the experimental results. Scaling analysis (with indicated in the paper assumptions) led to the Nusselt number correlation in the form of a power function of thermo-magnetic Rayleigh number. It was derived and shown that the Nusselt number is proportional to the thermo-magnetic Rayleigh number raised to a power of 0.25. The comparison with the experimental results gave good agreement and is promising for brief and quick estimation of heat transfer.

## 10. References

[1] Mallinson G D, Graham A D and de Vahl Davis G 1981 Three-dimensional Flow in a Closed Thermosyphon *J. Fluid Mech.* **109** 259-75
[2] Japikse D, Jallouk P A and Winter E R F 1971 Single-phase Transport Processes in the Closed Thermosyphon *Int. J. Heat Mass Tran.* **14** 869-87
[3] Ishihara I, Fukui T and Matsumoto R 2002 Natural Convection in a Vertical Rectangular Enclosure with Symmetrically Localized Heating and Cooling Zones *Int. J. Heat Fluid Fl.* **23** 366-72
[4] Lock G S H and Kirchner J D 1992 Some Characteristics of the Inclined, Closed Tube Thermosyphon under Low Rayleigh Number Conditions *Int. J. Heat Mass Tran.* **35 (1)** 165-73

[5] Honda K, Sato A and Nakabayashi S 2003 Magneto-taxis of Nonlinear Chemical Reaction *Proc. of the 7th Symp. on New Magneto-Science* (Tsukuba, Japan) 52-5
[6] Uyeda C, Tanak K, Sakakibara M and Takashima R 2003 Development of a Method to Detect Magnetic Anisotropy with High Sensitivity in Micro-Gravity Condition *Proc. of the 7th Proc. of the 7th Symp. on New Magneto-Science* (Tsukuba, Japan) 92-5
[7] Onodera H Jin Z and Chida S 2003 Human Body Risk Assessment Under High Magnetic field Environment *Proc. of the 7th Symp. on New Magneto-Science* (Tsukuba, Japan) 208-16
[8] Ozoe H 2005 *Magnetic Convection* (London: Imperial College Press)
[9] Simon M D and Geim A I 2000 Diamagnetic levitation: Flying frogs and floating magnets (invited) *J. Appl. Phys.* **87** 6200-4
[10] Wakayama N I, Okada T, Okano J and Ozawa T 2001 Magnetic promotion of oxygen reaction with Pt catalyst in sulfuric acid solutions *Jpn J. Appl. Phys.* **40** 269-71
[11] Bednarz T, Fornalik E, Tagawa T, Ozoe H and Szmyd J S 2006 Convection of paramagnetic fluid in a cube heated and cooled from side walls and placed below a superconducting magnet: comparison between experiment and numerical computations *Thermal Science and Engineering* **14** pp 107-114
[12] Kenjeres S, Pyrda L, Wrobel W, Fornalik-Wajs E and Szmyd J S 2012 Oscillatory states in thermal convection of a paramagnetic fluid in a cubical enclosure subjected to a magnetic field gradient *Phys. Rev. E* **85** 1-8
[13] Wrobel W, Fornalik-Wajs E and Szmyd J S 2010 Experimental and numerical analysis of thermo-magnetic convection in a vertical annular enclosure *Int. J. Heat Fluid Flow* **31** 1019-1031
[14] Fornalik E, Filar P, Tagawa T, Ozoe H and Szmyd J S 2006 Effect of magnetic field on the convection of paramagnetic fluid in the unstable and stable thermosyphon-like configurations *Int. J. Heat Mass Tran.* **49** 2642-51
[15] VDI-Wärmeatlas 1997 VDI-Verlag
[16] Braithwaite D, Beaugnon E and Tournier R 1991 Magnetically controlled convection in a paramagnetic fluid, *Nature* **354** 134-6
[17] Ozoe H and Churchill S W 1973 Hydrodynamic Stability and Natural Convection in Newtonian and Non-Newtonian Fluids Heated from Below, *AIChE Symposium Series, Heat Transfer* **69 (131)** 126-33
[18] Tagawa T, Shigemitsu R and Ozoe H 2002 Magnetizing force modeled and numerically solved for natural convection of air in a cubic enclosure: Effect of the direction of the magnetic field *Int. J. Heat Mass Tran.* **45** 267-77
[19] Filar P, Fornalik E, Tagawa T, Ozoe H and Szmyd J S 2006 Numerical and experimental analyses of magnetic convection of paramagnetic fluid in a cylinder *J. Heat Transf.* **128** 183-91.
[20] Mukhopadhyay A, Ganguly R, Sen S and Puri I K 2005 A scaling analysis to characterize thermomagnetic convection *Int. J. Heat Mass Tran.* **48** 3485-92

**Acknowledgement**
The present work was supported by the Polish Ministry of Science (Grant AGH No. 11.11.210.198).